Neuroprotective effects of an *in vitro* BBB permeable phenoxythiophene sulfonamide small molecule in glutamate-induced oxidative injury

SMRITEE POKHAREL[1], NAILYA S. GLIYAZOVA[1], SRINIVASA R. DANDEPALLY[1], ALFRED L. WILLIAMS[1,2] and GORDON C. IBEANU[1,2]

[1]Biomanufacturing Research Institute and Technology Enterprise (BRITE) and [2]Department of Pharmaceutical Science, North Carolina Central University, Durham, NC 27707, USA

Received March 29, 2021; Accepted October 18, 2021

DOI: 10.3892/etm.2021.11002

Abstract. Reactive oxygen species (ROS) play a central role in oxidative stress-associated neuronal cell death during ischemia. Further investigation into the inhibition of excessive ROS generation post-stroke is urgently required for the treatment of ischemic stroke. In the present study, the neuroprotective properties of the blood-brain barrier (BBB) penetrant B355227 were investigated. B355227 is a chemical analogue of B355252, and the role of the phenoxythiophene sulfonamide compound B355227 was further investigated in a glutamate-induced oxidative injury model. An *in vitro* model of the BBB was established in the immortalized mouse brain capillary endothelial cell line, bEnd.3. Formation of barrier in Transwell inserts was confirmed using EVOM resistance meter and Caffeine, Imatinib and Axitinib were used to validate the efficacy of the model. The validated BBB assay in combination with high performance liquid chromatography were used to analyse and verify the permeability of B355227 through the barrier. The integrity of the cell junctions after the BBB assays were confirmed using immunofluorescence to visualize the expression of the barrier junction protein zonula occludens-1. Cell survival was measured with Resazurin, a redox indicator dye, in HT22, a hippocampal neuronal cell treated with 5 mM glutamate or co-treated with the B355227 recovered from the BBB permeability experiment. Changes in glutathione levels were detected using a glutathione detection kit, while analyses of ROS, calcium (Ca^{2+}), and mitochondrial membrane potential (MMP) were accomplished with the fluorescent dyes 2',7'-dichlorofluorescein diacetate, Fura-2 AM and MitoTracker Red dyes, respectively. Immunoblotting was also performed to detect the expression and activation of Erk1/2, p-38, JNK, Bax and Bcl-2. The results of the present study demonstrated that B355227 crossed the BBB *in vitro* and protected HT22 from oxidative injury induced by glutamate exposure. Treatment of cells with B355227 blocked the glutamate-dependent depletion of intracellular glutathione and significantly reduced ROS production. Increased Ca^{2+} influx and subsequent collapse of the MMP was attenuated by B355227. Furthermore, the results of the present study demonstrated that B355227 protected against oxidative stress via the MAPK pathway, by increasing the activation of Erk1/2, JNK and P38, and restoring anti-apoptotic Bcl-2. Collectively, the results of the present study indicate that B355227 has potent antioxidant and neuroprotective attributes in glutamate-induced neuronal cell death. Further investigation into the role of B355227 in the modulation of glutamate-dependent oxidative stress is required.

Introduction

Stroke is the fifth leading cause of death in the United States, affecting >795,000 individuals each year (1). Elderly patients with underlying chronic and neurodegenerative conditions such as Alzheimer's and Parkinson's disease exhibit a higher risk of ischemic strokes that often lead to long term disability (2). Partial or complete blockage of the cerebral arteries during cerebral ischemia restricts blood flow and affects the metabolic needs of the brain (3). As a result, neuronal function is impaired and cell death occurs due to excessive glutamate, inadequate supply of oxygen and glucose, collapse in energy dependent processes, increase in reactive oxygen species (ROS) and disruption of the blood-brain barrier (BBB) (3,4).

Glutamate is an amino acid excitatory neurotransmitter involved in neuronal development, learning, memory and aging (5,6). However, high concentrations of glutamate released under pathologic stimuli overwhelms neurons and contributes to increased oxidative stress and neuronal damage (7). Glutamate

Correspondence to: Dr Gordon C. Ibeanu, Department of Pharmaceutical Science, North Carolina Central University, 1801 Fayetteville Street, Durham, NC 27707, USA
E-mail: gibeanu@nccu.edu

Abbreviations: BBB, blood-brain barrier; CM, conditioned media; GSH, glutathione; H2DCFDA, 2',7'-dichlorofluorescein diacetate; ROS, reactive oxygen species; TEER, trans-endothelial electrical resistance; ZO-1, zonula occludens-1

Key words: oxidative stress, glutamate, neuroprotection, *in vitro* BBB

neurotoxicity occurs when a high concentration of extracellular glutamate inhibits the glutamate/cystine antiporter, lowering the level of cystine in the cell. Cystine is the precursor of glutathione (GSH), and upon depletion, elevates intracellular ROS resulting in oxidative stress (8). Accumulation of ROS leads to an increase in the level of Ca^{2+} in the mitochondrial matrix (9). High levels of Ca^{2+} sensitizes the formation of the mitochondrial permeability transition pore (MPTP), leading to the collapse of the mitochondrial membrane potential (MMP) and cell death (9-11). Furthermore, binding of glutamate to the corresponding receptors activates downstream signalling pathways, such as the MAPK signalling pathway, which serves a central role in neuronal plasticity, survival, death and memory formation (12). Moreover, an increase in Erk1/2 mediated by ROS further exacerbates neurotoxicity (13). In contrast, a previous study reported that Erk1/2 serves a key role in the survival of neurons during post ischemic recovery (13,14). Perturbation of cellular Ca^{2+} homeostasis and increased oxidative stress activates the JNK and p38 signalling pathways, and promotes neuronal cell death (15).

B355252, a phenoxythiophene sulfonamide compound, exerts a number of neuroprotective effects. It was initially identified from a proprietary library of chemical compounds as a potentiator of nerve growth factor (NGF)-primed neurite outgrowth and elongation in a neuronal cell model (16). In the presence of sub-physiological concentrations of NGF, B355252 promotes differentiation and production of axon-like processes in pheochromocytoma cell line PC12, and its derivative neuroscreen-1 (16). Previous studies have reported the anti-apoptotic and antioxidant properties of B355252 in chemical models of ischemia and Parkinson's disease *in vitro* (17-19). In the present study, B355227 (molecular weight, 494.3 DA), a substituted analogue of B355252, synthesized by our medicinal chemists during the SAR studies of B355252, was shown to readily cross the BBB in an *in vitro* assay. B355227 exerted neuroprotective effects in a glutamate-induced oxidative stress model, and protected HT22 cells from oxidative stress via the modulation of a number of key effectors, such as GSH, ROS and Ca^{2+} overload. In addition, B355227 downregulated the activation of Erk1/2, JNK and P38 protein families that were reported to serve key roles in ischemia (18).

Materials and methods

Cell culture. Mouse hippocampal HT22 and endothelial bEND.3 cell lines were purchased from the American Type Culture Collection. Cells were maintained at 37˚C in growth media (GM) consisting of DMEM (Cytiva) supplemented with 10% FBS (Cytiva), 1% penicillin/streptomycin (Cytiva) and 1% L-glutamine (Lonza Group, Ltd.) in a humidified incubator with 5% CO_2. For all experiments, cells were incubated at 37˚C in a humidified incubator with 5% CO_2, unless indicated otherwise.

Nuclear Magnetic Resonance (^1H and ^{13}C) of B355227. B355227 was synthesized and characterized by the Medicinal Chemistry Group, Department of Pharmaceutical Science, North Carolina Central University (Durham, USA). All solvents and reagents were obtained from commercial sources (16). Proton nuclear magnetic resonance (1H NMR) spectra and carbon nuclear magnetic resonance (13C NMR) spectra were recorded on a Varian VNMRS-500 (500 MHz) spectrometer.

Assessment of cell viability. Cell viability was assessed using the redox indicator dye resazurin sodium salt (Sigma-Aldrich; Merck KGaA). HT22 cells were seeded in 96-well plates at a density of $2x10^4$ cells/well and incubated overnight at 37˚C. Next day, the cells were treated with drugs (B355227 with and without glutamate) in GM at 37˚C for 24 h. Resazurin was added to the wells to a final concentration of 1%, and cells were incubated at 37˚C for 3 h. Fluorescence was measured using a PHERAstar microplate reader (BMG Labtech), at an excitation wavelength of 540 nm, and an emission wavelength of 590 nm.

Measurement of trans-endothelial electrical resistance (TEER). bEND.3 cells were seeded at a density of $1.3x10^6$ cells/well in Transwell inserts and cultured for 12 days in GM at 37˚C in 5% CO_2. The TEER was measured daily using End-Ohm chopstick electrodes connected to an EVOM resistance meter (World Precision Instruments, Inc.). The TEER value of each well was calculated by subtracting the resistance of blank inserts without cells from the sample inserts with cells. Values were expressed as $\Omega\ cm^2$.

Evaluation of in vitro barrier function. Following the incubation of bEND.3 cells in Transwell inserts for 12 days as previously described, cells were washed and incubated in serum-free media (SFM) containing DMEM, 1% L-glutamine and 1% penicillin/streptomycin for 1 h at 37˚C. SFM was replaced with 1 ml of 1X Hanks' Buffered Saline Solution (HBSS; Lonza) at the apical and luminal sides of the Transwell insert, followed by exposure to vehicle or 100 μg/ml Fluorescein isothiocyanate-dextran (FITC-dextran ; 40 kDa; Sigma-Aldrich; Merck KGaA) at 37˚C for 1 h. After incubation, media from the luminal side of the Transwell insert was collected and the fluorescence was measured using spectrophotometry at an excitation wavelength of 485 nm, and an emission wavelength of 520 nm. Subsequently, 20 μM Caffeine (molecular weight, 194 kDa), a low molecular weight compounds known to be permeable, and 20 μM Imatinib (molecular weight, 493 kDa) and 20 μM Axitinib (molecular weight, 389 kDa), compounds known to be impermeable to the BBB were used to further validate the assay. Briefly, after 14 days in culture of homogeneous bEND.3 monolayer culture and formation of BBBs, as assessed by TEER value using End-Ohm chopstick electrodes connected to an EVOM resistance meter, were pre-incubated in SFM at 37˚C for 1 h, which was subsequently replaced with 1 ml of 1X HBSS in both chambers of the Trans-well plates. Vehicle or 20 μM of caffeine, imatinib and axitinib were added to the cells and incubated at 37˚C. Samples were collected from the luminal side at 1, 2 and 3 h, vacuum dried and dissolved in 300 μl of high-performance liquid chromatography (HPLC) grade ultra-pure distilled water for further analysis.

HPLC analysis. A total of 40 μl of luminal side HBSS sample collected after exposure of bEND.3 cells to B355227 were analyzed at room temp (22˚C) using Agilent 1220 Infinity II LC reverse-phase system detector (Agilent Technologies, Inc.) with diode array variable wavelength (190-600 nm).

Separation of analytes was achieved in mobile phase consisting of 10 to 95% acetonitrile/H_2O with 0.1% formic acid, at a flow rate of 0.5 ml/min for 7 min on Waters Sunfire OBD using C18 column (3x100 mm; 5 μM; Waters Corporation).

Compound permeability assay. An *in vitro* BBB permeability assay was performed using bEND.3 cells that had been incubated in Transwell inserts for 12 days as previously described, when maximum TEER was observed in culture. Cells were treated with vehicle or 20 μM B355227 (determined using a dose response toxicity assay) in 1 ml GM at the apical side of the chamber. A total of 1 ml GM was added to the luminal side of the chamber and incubated for 1 h at 37˚C in 5% CO_2. Following incubation, media from the luminal side was retrieved and centrifuged at room temp for 10 min at 150 x g to remove cell debris. The supernatant was referenced as conditioned media (CM) and was used in further neuroprotection assays.

Immunofluorescence. Following the BBB permeation assay in bEND.3 cells, expression of zonula occludens-1 (ZO-1) protein was analyzed using immunofluorescence, as previously described (20). Cells employed in the permeability assay were washed with PBS and fixed in 4% formaldehyde at room temp for 15 min. The cells were blocked in 10% donkey serum (Rockland Immunochemicals, Inc.) for 1 h at room temp and incubated overnight at 4˚C with anti-rabbit anti-ZO-1 antibody (1:1,000; cat. no. 40-2200; Thermo Fisher Scientific, Inc.) diluted 200-fold. Following primary incubation, the cells were washed with PBS and incubated with Alexa Fluor 488-conjugated donkey anti-rabbit IgG secondary antibody (1:1,000; cat. no. A21206; Thermo Fisher Scientific, Inc.) room temperature for 1 h. Cells were washed three times with PBS and mounted on slides with VECTASHIELD (Vector Laboratories, Inc.). Images of the stained cells were captured using a FV3000 confocal laser scanning microscope (magnification, x40; Olympus Corporation).

Neuroprotection assay with CM. HT22 cells ($2x10^4$ cells/well) grown overnight at 37˚C in 96-well plates were exposed to 100 μl CM in the presence or absence of 5 mM glutamate (Sigma-Aldrich; Merck KGaA). Following 24 h incubation at 37˚C in 5% CO_2, cell viability was assessed using the resazurin assay, as previously described.

Analysis of GSH. Determination of reduced GSH was performed as described by Gliyazova *et al* (18) using MCB glutathione detection kit (cat. no. 30019; Biotium, Inc.). Briefly, a total of $6.5x10^5$ HT22 cells grown overnight at 37˚C in 64-mm plates were treated with B355227 with and without glutamate for 24 h. Cells were subsequently counted, and $1x10^6$ cells were lysed and centrifuged at 700 x g for 5 min at 22˚C. A total of 5 μl cell lysate was mixed with 5 μl of 10 mM MCB and 2 μl of glutathione-S-transferase (GST) reagent according to the protocol provided with the MCB glutathione detection kit, followed by 30 min incubation at 37˚C. Fluorescence was measured using a PHERAStar multipurpose fluorescence reader (BMG LabTech GmbH) at an excitation wavelength of 394 nm, and an emission wavelength of 490 nm.

Determination of ROS. Intracellular ROS was determined using 2',7'-dichlorofluorescein diacetate (H_2DCFDA; cat. no. D399; Thermo Fisher Scientific, Inc.). A total of $2x10^4$ HT22 cells were cultured overnight at 37˚C in 96-well plates and treated with B355227 in the presence or absence of glutamate for 8 h. The cells were subsequently washed with phosphate buffered saline (PBS) and incubated with 10 μM H_2DCFDA in phenol red-free DMEM (cat. no. 21063029; Thermo Fisher Scientific, Inc.) for 30 min at 37˚C. Cells were washed again in PBS and the fluorescence was measured using a PHERAStar microplate reader (BMG LabTech) at an excitation wavelength of 485 nm, and an emission wavelength of 520 nm. After the fluorometric measurements, the cells were lifted from each well using trypsin-EDTA (Thermo Fisher Scientific, Inc.) and counted in the Vi-CELL XR cell viability analyser (Beckman Coulter, Inc.) to determine the total number of cells. The data was normalized by dividing the total fluorescence intensity at every time-point by the total number of cells.

Measurement of Ca^{2+}. Changes in intracellular Ca^{2+} levels were measured fluorometrically using Fura-2 AM dye (cat. no. 47989; Sigma-Aldrich; Merck KGaA). HT22 cells were seeded at $6.5x10^5$ in 64-mm plates and cultured overnight at 37˚C were treated with B355227 with and without glutamate for 24 h at 37˚C. Following incubation, the cells were detached with trypsin-EDTA, counted in the Vi-CELL and $1x10^6$ cells from each treatment group (untreated control, glutamate, B355227 and B355227 + glutamate groups) were incubated with 2.5 M Fura-2 AM in phenol red-free DMEM (cat. no. 21063029; Thermo Fisher Scientific, Inc.) for 30 min at 37˚C. Cells were washed with PBS, resuspended in phenol-free DMEM containing 10% FBS and incubated at 37˚C. After 30 min incubation, cells were sequentially excited at 340 and 380 nm using a Fluoromax-4 spectrofluorometer (HORIBA Scientific) and the peak emission signal was measured at 510 nm. Changes in Ca^{2+} concentration were measured using the ratio of the emission signals obtained, and the results were interpreted as relative values.

Measurement of the MMP. HT22 ($6x10^6$ cells) cultured overnight at 37˚C on cover slips and exposed to 5 μM B355227 (Medicinal Chemistry Group, North Carolina Central University) with and without 5 mM glutamate (Sigma-Aldrich; Merck KGaA) were treated with 200 nM MitoTracker Red CMXRos dye (Thermo Fisher Scientific, Inc.) in SFM for 30 min at 37˚C. The cells were washed with PBS and re-incubated in GM for 15 min at 37˚C. Following incubation, the cells were fixed with 4% formaldehyde in PBS for 15 min at room temp, and cell nuclei were stained with 10 μg/ml DAPI in PBS for 5 min at room temp. Cover slips were mounted on the slides and images were captured using a Zeiss LSM-800 confocal scanning microscope (Zeiss GmbH) at an excitation wavelength of 579 nm, and an emission wavelength of 599 nm (magnification, x60). The images were analysed with ImageJ software, version 1.52 (National Institutes of Health), and the fluorescence intensity normalized as follows: Corrected total fluorescence (CTCF)=integrated density - (area of collected cell x mean fluorescence of background reading).

Immunoblot analysis. Immunoblots were performed according to a previous study by Pokharel *et al* (21). Briefly, HT22 cells ($1x10^7$) treated for 24 h at 37˚C with 5 mM glutamate

supplemented with or without 5 μM B355227 were lysed in RIPA buffer containing protease inhibitor cocktail (Thermo Fisher Scientific, Inc.). The protein content was quantified using a Pierce BCA protein assay kit (Thermo Fisher Scientific, Inc). A total of 30 μg protein were electrophoresed on 4-12% SDS-PAGE and transferred to PVDF membranes. The membranes were subsequently blocked with Intercept (PBS) blocking buffer (cat. no. 927-70001; LI-COR Biosciences) for 1 h at room temp and incubated overnight at 4˚C with the following primary antibodies obtained from Cell Signaling Technology, Inc.: Anti-Erk1/2 (1:1,000; cat. no. 4695), anti-phospho-Erk1/2 (1:2,000; cat. no. 9106), anti-p38 (1:1,000; cat. no. 8690), anti-phospho-p38 (1:2,000; cat. no. 9216), anti-JNK (1:1,000; cat. no. 9252), anti-phospho-JNK (1:2,000; cat. no. 9255), anti-Bax (1:1,000; cat. no. 2772), anti-Bcl-2 (1:1,000; cat. no. 3498) and anti-β-actin (1:1,000; cat. no. 3700) as reference protein. The membranes were rinsed four times for 5 min at room temperature in 1X TBST (0.2% Tween-20) and incubated at room temperature with 15,000-fold dilution of IRDye 800CW-conjugated donkey anti-rabbit IgG (cat. no. 926-32213; LI-COR Biosciences) or 20,000-fold dilution of IRDye 680LT-conjugated donkey anti-mouse IgG (cat. no. 926-68022; LI-COR Biosciences) for 1 h. The membranes were rinsed four times in 1X TBST for 5 min, and finally in 1X TBS to remove residual Tween-20. Images were captured using an Odyssey IR imaging system and signals were analysed using Odyssey 2.0 software (LI-COR Biosciences).

Statistical analysis. Statistical analyses were performed in GraphPad Prism version 7 (GraphPad Software, Inc.). Data are presented as the mean ± standard deviation of at least three biological replicates in at least three independent experiments. Significant differences between groups were determined using one-way ANOVA followed by Tukey's multiple comparisons post hoc test. $P<0.05$ was considered to indicate a statistically significant difference.

Results

Structural characterization of B355227. Synthesis of B355227, a substituted analogue of B355252 was confirmed by NMR. Chemical shifts (δ) are reported in parts per million (ppm) using tetramethylsilane as an internal standard (spectral data not shown). Multiplicities were reported using the following abbreviations: Br, broad; s, singlet; d, doublet; t, triplet; q, quartet; m, multiplet. 1H NMR (CDCl3, 500 MHz) δ 2.97 (t, 4H, J=5.0 Hz), 3.12 (t, 4H, J=5.0 Hz), 3.76 (s, 3H), 4.18 (s, 2H), 6.52 (dd, 1H, J=2.0, 8.0 Hz), 6.64 (t, 1H, J=2.0 Hz), 6.73 (dd, 1H, J=2.0, 8.5 Hz), 6.76 (s, 1H), 6.78-6.83 (m, 2H), 7.22 (ABq, 2H, J=8.5 Hz), 7.28 (s, 1H); 13C NMR (CDCl3, 125 MHz) δ 45.7, 47.4, 49.5, 55.2, 105.2, 107.9, 111.2, 112.6, 113.4, 113.6, 120.1, 128.2, 129.8, 130.3, 130.7, 137.4, 153.3, 158.2, 158.7, 159.9. The values indicate estimated chemical shift numbers of ^{1}H and ^{13}C of B355227 in parts per million (ppm).

B355227 is permeable across bEND.3 cells in vitro. An *in vitro* permeability assay was performed to determine the permeability of B355227 through the bEND.3 BBB monolayer assay system. TEER was initially measured prior to the permeability experiments to ensure model barrier integrity. Expression levels of the ZO-1 protein were analyzed using immunofluorescence to ensure cell confluency. A gradual and significant rise in TEER values was observed after 10 days in culture compared with day 8, attaining a maximum of 50 Ω cm^2 on day 12, which remained at a high level until day 16, and thereafter declined on day 18 (Fig. 1A). TEER is a measure of electrical resistance in cells and reflects the formation of functional barriers. A rise in TEER value is associated with an increase in claudin-5 and ZO-1 expression at the contact points between cells (22). Immunofluorescence detected similar pattern of ZO-1 localization on the membrane contact points of bEND.3 cells treated with B35227 compared with untreated control, which confirmed the integrity of tight junctions in the cells treated with 20 μM B355227 (Fig. 1E).

The maximum nontoxic dose of B355227 in bEND.3 cells was established by evaluating the viability of the cells after treatment with varying concentrations (2.5-40 μM) of the compound for 24 h. B355227 exhibited no adverse effect on bEND.3 cells at concentrations up to 20 μM, but exhibited dose-dependent toxicity at concentrations ≥30 μM (Fig. 1B). Following the establishment of the highest non-toxic concentration of B355227 as 20 μM, the permeability assay was performed to determine the capacity of B355227 to cross the bEND.3 BBB. B355227 was detected in the luminal chamber using HPLC (Fig. 1C), and a time-dependent increase in compound concentration in the luminal component of the Transwell plate was observed (Fig. 1D). A total of ~8 μM of B355227 was recovered in the luminal side of the Transwell after 1 h exposure of cells to 20 μM of B355227 compared with samples taken after addition of the compound without incubation (Fig. 1D). The quantity recovered increased to 9 μM and 12 μM at 2 and 3 h, respectively (Fig. 1D). Following the permeability assay, the cells were stained with anti-ZO-1 antibody to confirm that detection of B355227 in the luminal side was a result of diffusion or paracellular transport across the membrane and not due to a compromised or leaky membrane. No difference was observed in the levels of ZO-1 expression in the control group compared with the drug treated cells, which indicated the passage of B355227 through the BBB in the experimental model (Fig. 1E).

B355227 protects against glutamate-induced toxicity. The neuroprotective effect of B355227 against glutamate-induced toxicity was assessed in HT22 cells. The IC_{50} of glutamate was established in HT22 cells to determine the optimal concentration required for subsequent experiments. The IC_{50} of glutamate in the cell line was 5.96 mM (Fig. 2A). Thus, cells were treated with increasing concentrations of B355227 (2.5, 5 and 10 μM) in the presence of 5 mM glutamate, and assessed for retention of viability. The results of the present study demonstrated that 5 mM glutamate significantly reduced the viability of HT22 cells by 40% compared with untreated control (Fig. 2B). Following co-treatment of 2.5, 5 or 10 μM B355227 with 5 mM glutamate, there was a significant dose-dependent increase in cell viability by 10, 30 and 10%, respectively, compared with cells treated solely with glutamate (Fig. 2B). Furthermore, to validate the bioactivity of B355227, HT22 cells were treated with CM recovered from the luminal side of the assay chamber following the B355227 permeability assay, in the presence or absence of 5 mM glutamate. Cells exposed to glutamate in CM

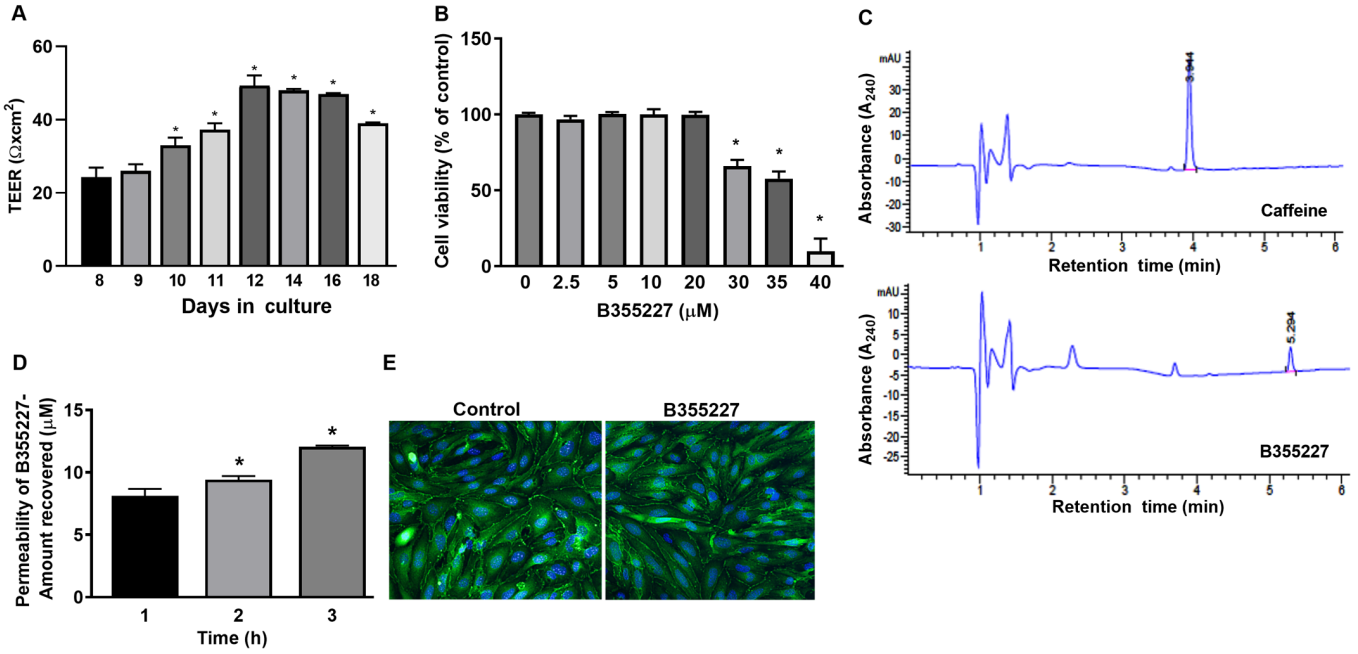

Figure 1. Analysis of the passage of B355227 through an in vitro BBB model. (A) Confirmation of barrier establishment using TEER. bEND.3 cell cultured in Transwell inserts demonstrated a gradual and significant rise in TEER over several days in culture. *P<0.05 vs. 8 day group. (B) Cells treated with different concentrations of B355227 following the formation of the barrier revealed no adverse effects of B355227 at concentrations up to 20 μM. *P<0.05 vs. control group. (C) HPLC chromatograms demonstrate the detection of caffeine and B355227 following the permeability assay. (D) B355227 permeability assay revealed a time-dependent increase in the passage of B355227 as measured using HPLC. *P<0.05 vs. 1 h group. (E) Immunofluorescent staining of the tight junction protein ZO-1 confirms integrity of the barrier following the permeability assay. Continuous expression of ZO-1 (green) was observed along the cytoplasmic border of cells and central nuclei (blue) following implementation of the BBB permeability assay. Magnification, x40. Data are presented as the mean (n=3) ± standard deviation, obtained from three independent experiments. BBB, blood-brain barrier; TEER, trans-endothelial electrical resistance; HPLC, high-performance liquid chromatography; ZO-1, zonula occludens-1.

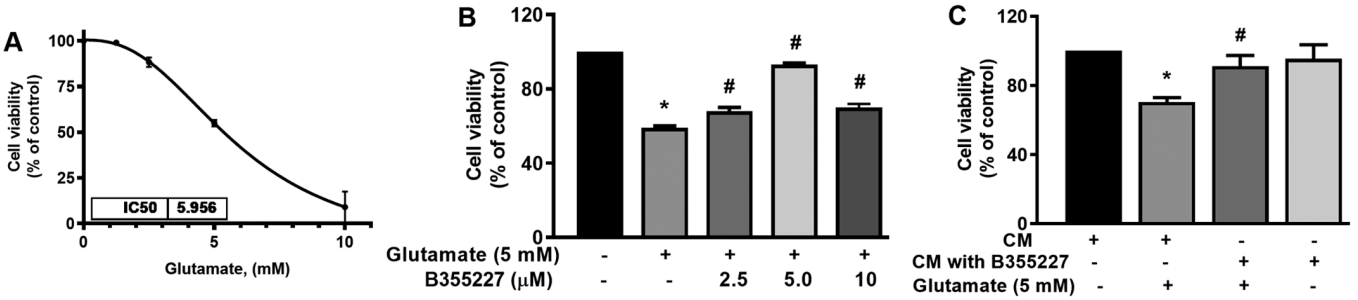

Figure 2. B355227 crosses the BBB and mediates protection of HT22 neurons in a glutamate-induced cell death model. (A) Determination of the concentration of glutamate that reduces HT22 cell viability by 50% (n=6). (B) Effects of B355227 on glutamate-induced cell viability. Co-treatment of cells with B355227 and glutamate protected HT22 neurons from glutamate-induced toxicity. (C) Confirmation of BBB permeability and the biological activity of B355227. Cells were treated with CM for 1 h in presence or absence of 5 mM glutamate. B355227 CM significantly increased cell viability in the presence of glutamate. Data are presented as the mean (n=3) ± standard deviation obtained from three independent experiments. *P<0.05 vs. control group; #P<0.05 vs. glutamate treated group. BBB, blood-brain barrier; CM, conditioned media.

demonstrated an increased survival of ~20% compared with the cells treated with glutamate alone (Fig. 2C). Furthermore, cells exposed to B355227 CM for 24 h revealed no evidence of toxicity, and no significant difference was observed in cell viability compared with cells exposed to the control CM.

B355227 increases GSH, reduces ROS and Ca^{2+}, and blocks dissipation of the MMP in HT22 cells. The cellular mechanisms underlying the protective actions of B355252 in HT22 cells undergoing glutamate-induced oxidative stress were investigated. GSH, an antioxidant that plays a role in scavenging ROS in response to oxidative stress (23) was quantified. The results of the present study revealed a significant decrease of ~40% in cellular glutathione content following exposure to glutamate for 24 h, compared with the untreated control cells (Fig. 3A). In the presence of B355227, the decline in GSH triggered by glutamate treatment was substantially mitigated, while the compound alone exhibited no effect on GSH compared with the control cells (Fig. 3A). As GSH serves a key role in the detoxification of H2O2 and modulates ROS (24), ROS levels in cells was investigated using the oxidative stress indicator, H_2DCFDA. The results of the present study indicated a 1.4-fold increase in ROS accumulation in cells exposed to glutamate, compared with the untreated cells (Fig. 3B). Treatment with

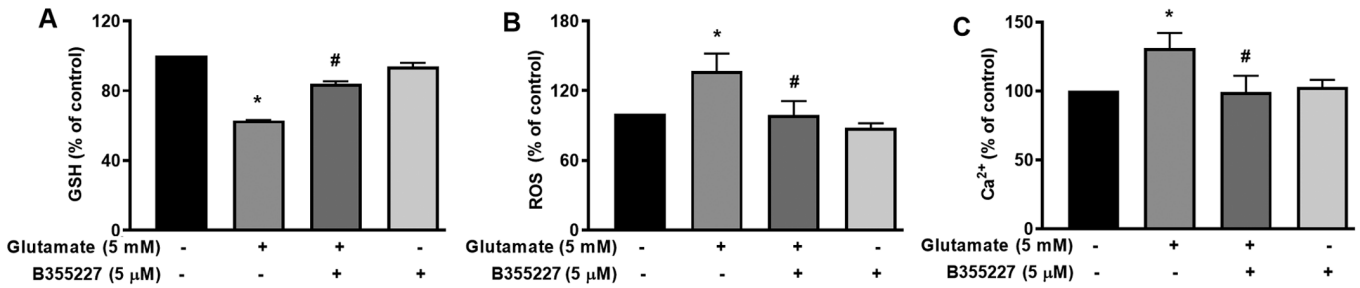

Figure 3. Effects of B355227 on glutamate-induced oxidative stress in HT22 cells. Control cells and cells treated with glutamate in the presence or absence of B355227 were assessed for levels of GSH, ROS and Ca^{2+}. (A) Measurement of GSH level. Cells co-treated with B355227 demonstrated a significant increase in the levels of GSH. (B) Evaluation of intracellular ROS. Glutamate-induced increase in intracellular ROS was suppressed following treatment with B355227. (C) Measurement of intracellular Ca^{2+}. Glutamate-induced increase in intracellular Ca^{2+} was suppressed following treatment with B355227. Data are presented as the mean (n=3) ± standard deviation obtained from three independent experiments. *P<0.05 vs. control group; $^{\#}$P<0.05 vs. glutamate treated group. GSH, glutathione; ROS, reactive oxygen species.

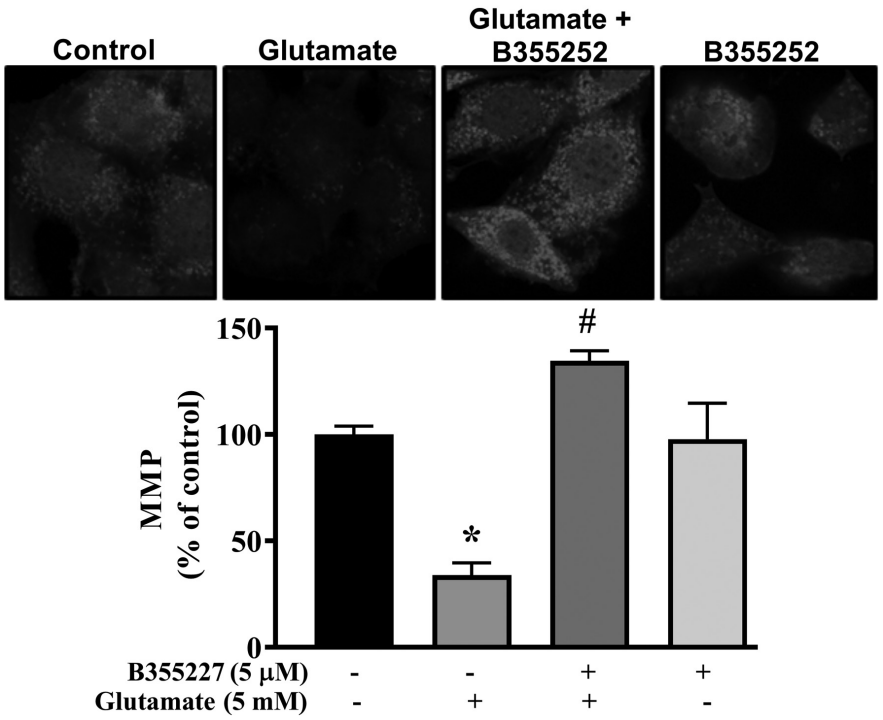

Figure 4. Effects of B355227 on the glutamate-dependent collapse of the MMP. The integrity of the MMP was determined in HT22 cells treated with glutamate in the presence or absence of B355227. Confocal images demonstrating the collapse of the MMP induced by glutamate are represented by a decrease in cellular fluorescence (center left) and protection of the MMP by B355227 is represented by markedly increased fluorescence (center right). Magnification, x40. Bars represent densitometric quantification of the corresponding images. The data are presented as the mean (n=3) ± standard deviation obtained from three independent experiments. *P<0.05 vs. control group; $^{\#}$P<0.05 vs. glutamate treated group. MMP, mitochondrial membrane potential.

5 μM B355227 considerably reduced the glutamate-induced increase of ROS by ~1.4-fold, which suggested that B355227 possessed antioxidant activity.

The mutual interplay of ROS and Ca^{2+} signalling serves a crucial role in controlling functional changes that accompany a number of pathophysiological events that include cellular dysfunction leading to neurodegenerative disorders, cardiovascular diseases and cancer (25,26). Therefore, to determine whether B355227 exerted its neuroprotective effects through modulation of Ca^{2+}, HT22 cells were exposed to glutamate alone or in conjunction with B355227. Following exposure to glutamate, the intracellular Ca^{2+} levels increased by ~25%, compared with the control cells (Fig. 3C). However, when co-treated with B355227, the glutamate-dependent increase in Ca^{2+} was attenuated, and the intracellular Ca^{2+} levels returned to a level comparable to those observed in untreated cells (Fig. 3C).

Collapse of the MMP is associated with cell death in glutamate-induced oxidative injury (27). Thus, the MMP in HT22 cells exposed to glutamate with or without B355227 was investigated using MitoTracker Red CMXRos dye. Exposure of HT22 cells to glutamate resulted in significant disruption of the MMP, indicated by a ~60% decrease in fluorescence intensity compared with untreated control cells (Fig. 4). In contrast, the signal intensity of the mitochondrial dye was concentrated at a significantly high level in cells co-treated with glutamate and B355227 compared to cells treated with glutamate alone. Similar values of fluorescence intensity were observed in cells treated with B355227 alone and the untreated control cells.

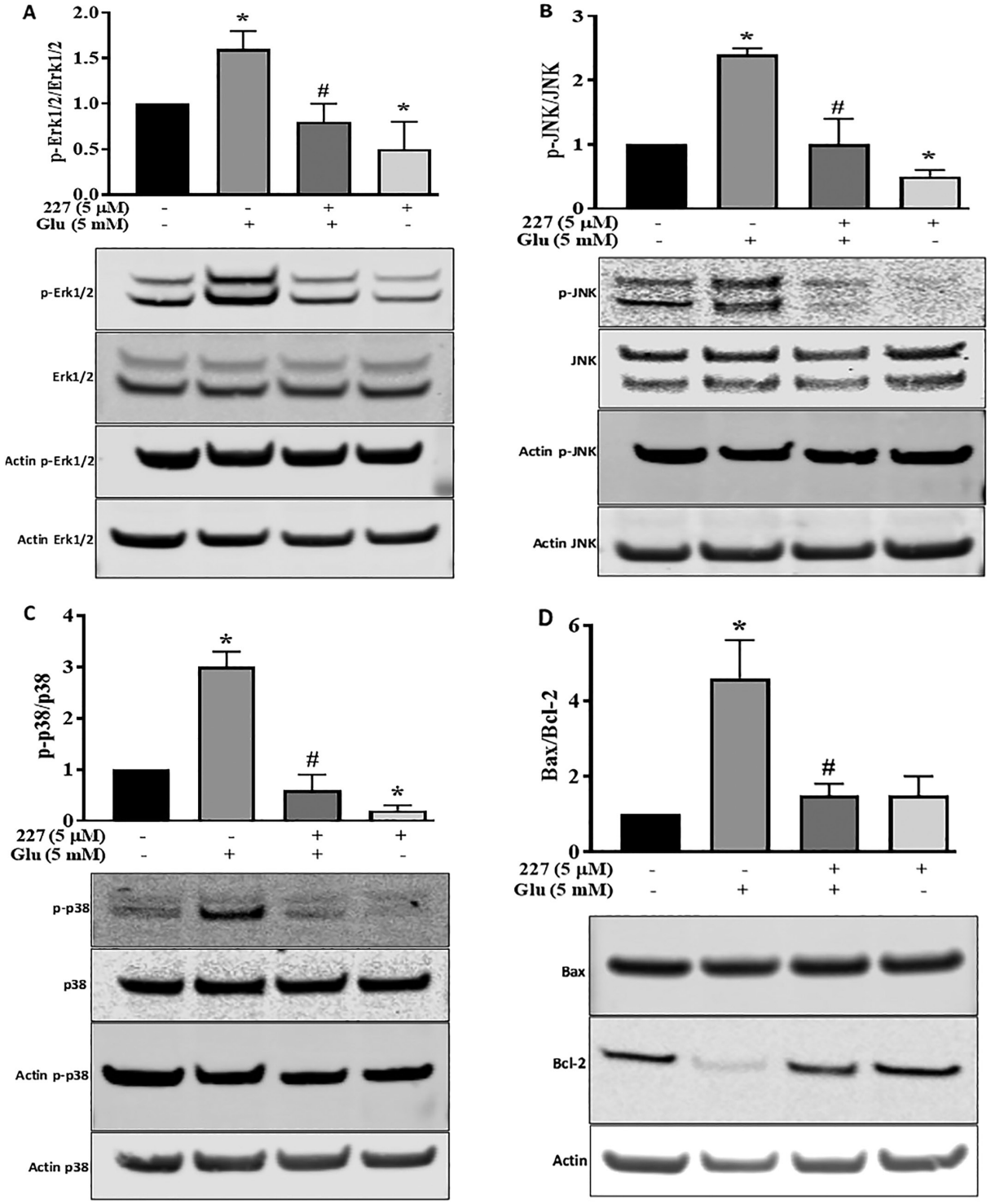

Figure 5. B355227 attenuates the effects of glutamate on the phosphorylation of the MAPK protein family and enhances the expression levels of Bcl-2. Western blots were performed on HT22 cells treated with glutamate in the presence or absence of B355227, and the levels of phosphorylated and total MAPK proteins were quantified using band densitometry. Double bands of Erk1/2 and JNK were measured. Protein expression levels of (A) Erk1/2 and p-Erk1/2, (B) JNK and p-JNK, (C) p38 and p-p38 and (D) the ratio of pro-apoptotic Bax and Bcl-2. Data are presented as the mean (n=3) ± standard deviation obtained from three independent experiments. *P<0.05 vs. to control; #P<0.05 vs. glutamate treated group. p-, phosphorylated.

Influence of B355227 on MAPK and Bax/Bcl-2 signalling pathways. Proteins of the MAPK family serve a dynamic role in glutamate-induced oxidative stress (28). To further explore the neuroprotective effects of B355227 following glutamate treatment, the MAPK pathway was investigated. The phosphorylation of Erk1/2, JNK and p38 proteins, along with the expression levels of pro-apoptotic Bax and anti-apoptotic Bcl-2 proteins were determined. Quantitative analysis of western blotting bands demonstrated a significant increase in Erk1/2 phosphorylation induced by glutamate, compared with the untreated control HT22 cells. However, the increase in Erk1/2 phosphorylation was reversed following co-incubation with glutamate and B355227 (Fig. 5A). Incubation of HT22 cells with B355227 alone exhibited no difference in the

phosphorylation of Erk1/2 compared with cells co-treated with glutamate and B355227, but significantly decreased the phosphorylation of Erk1/2 compared with untreated cells.

The involvement of JNK and p38 pathways in ischemia have been previously reported (29). Therefore, the expression levels and phosphorylation of JNK and p38 in HT22 cells were determined following treatment with either glutamate or B355227 alone, or in combination. Glutamate exposure increased the phosphorylation of JNK by 2.3-fold, and exposure to B355227 diminished the phosphorylation of JNK in the presence of glutamate (Fig. 5B). Similarly, glutamate treatment elevated P38 the phosphorylation, which was reduced below the basal level when treated in combination with B355227 (Fig. 5C). Interestingly, when HT22 was treated with B355227 alone the phosphorylation of JNK was reduced by ~2-fold, and the phosphorylation of p38 was reduced by a factor >5-fold, compared with the untreated control cells respectively (Fig. 5B and C).

The results of the present study indicated that an improvement in neuronal viability following treatment with B355227 was associated with a reduction in the glutamate-induced increase of intracellular Ca^{2+}, protection of mitochondrial potential and decreased MAPK pathway activation. Thus, the effects of B355227 on anti-apoptotic Bcl-2 and pro-apoptotic Bax proteins were investigated. The results demonstrated that treatment with glutamate alone reduced the expression levels of Bcl-2, but exerted no effects on the expression levels of Bax, resulting in a 4.2-fold increase in the pro-apoptotic Bax/Bcl-2 ratio compared with untreated cells (Fig. 5D). In contrast, the glutamate-induced reduction in Bcl-2 was abolished following co-treatment with glutamate and B355227, leading to ~4-fold decrease in the Bax/Bcl-2 ratio, similar to the observed Bax/Bcl-2 ratio in the control group. Treatment with B355227 alone increased the expression levels of Bcl-2 and Bax compared with the untreated controls. However, the ratio of pro-apoptotic Bax/Bcl-2 remained at a similar level to the ratio observed in the control group (Fig. 5D).

Discussion

Restricted passage of drugs through the BBB limits the choice of drug for the treatment of neurodegenerative diseases, and presents a major challenge for the development of new drugs targeting these disorders (30). The endothelial lining of cerebral micro-vessels controls the paracellular permeability of solute across the membrane and selectively allows the passage of compounds via transmembrane diffusion, absorption endocytosis or saturable transporters (31). An *in vitro* BBB model is being utilized for the screening of drugs that have the potential to permeate the BBB *in vivo* (22). In the present study, a bEND.3 monolayer in an *in vitro* BBB model was established to screen a series of analogues of B355252 (16), a phenoxythiophene compound. Confirmation of chemical structure is an important step in compound synthesis workflow, because it verifies information about the structure of organic molecules. One compound, B355227 identified from the series was permeable through the BBB *in vitro* and possessed neuroprotective properties. The structure was confirmed by proton and carbon NMR spectral analyses, which substantiated the positions of its proton and carbon peaks, and thus established the structural identity of the compound. Using the experimental model of the BBB in the present study, a TEER value of ~50 $\Omega\,cm^2$ was established. A wide range of variation in TEER values have been reported in previous studies, ranging from 30-140 $\Omega\,cm^2$ in bEND.3 cells (32,33). However, the present study demonstrated that the attained TEER value of ~50 $\Omega\,cm^2$ was sufficient to exclude the passage of low molecular weight imatinib and axitinib. Additionally, the results of Transwell assays demonstrated that visualization of continuous ZO-1 expression in the cytoplasmic border of bEND.3 cells highlighted the formation of proper tight junctions between cells in the Transwell culture system. ZO-1, claudin, occludin and junctional adhesion protein form a multiprotein complex with gap junction and adherence junction proteins, and play a central role in maintaining membrane integrity (34). The importance of ZO-1 in the formation of notochord, neuronal tube and allantois has been identified in a knockdown study using mice (35).

Hypoxia and glucose deprivation in ischemia initiates a complex cascade of molecular events including depletion of GSH, elevated ROS and an increase in Ca^{2+} influx (36). Oxidative stress-mediated elevation of ROS has been highlighted as a major contributor of glutamate-induced oxidative injury (37). The results of the present study demonstrated that B355227 protected HT22 cells from glutamate-induced cell injury, with an optimal concentration ~5 μM. Although there was significant protection at 10 μM B355227 compared with glutamate-only treated cells, cell viability was reduced when compared with cells treated with 5 μM B355227. The specific mechanisms underlying the decrease in cell viability are yet to be elucidated, as cells treated with B355227 alone demonstrated no toxicity at a concentration of 20 μM. We hypothesized that increasing the amount of B355227 to 10 μM in the presence of a high concentration of glutamate increased the stress burden on the metabolic activity of cells, and interfered with the antioxidant capacity of B355227, thus leading to a loss of effectiveness in cell protection.

Results of the present study demonstrated that the levels of ROS decreased in glutamate-treated cells as early as 8 h following treatment with B355227. In addition, B355227 prevented the glutamate-induced reduction of GSH, demonstrating the antioxidant and neuroprotective properties of the compound. A decrease in the cellular levels of GSH leads to the accumulation of mitochondrial ROS and Ca^{2+} overload, thus contributing to cell death, which is prevented by increasing the intracellular GSH (38). Similarly, inhibition of the Ca^{2+} channel is often used in the treatment of stroke, as it protects cells from glutamate-induced oxidative stress (39,40). The results of the present study also demonstrated markedly reduced levels of Ca^{2+} in cells exposed to glutamate in the presence of B355227, which indicates a role for B355227 in mitigating the elevation of Ca^{2+} during glutamate toxicity. Furthermore, an increase in mitochondrial Ca^{2+} during ischemia has been associated with the collapse of the MMP, involving poly (ADP-ribose) polymerase in the early phase, and formation of the MPTP in the late phase (41). Increase in the MPTP causes rupture in the outer mitochondrial membrane, releasing apoptosis inducing factor (AIF) from the inner mitochondrial space (42). Moreover, inhibition of glutamate-dependent MMP depolarization using B355227 involves AIF-1, as observed in our previous study using B355252 (18). Although both caspase-dependent and

-independent pathways have been proposed in glutamate-mediated toxicity, contrasting findings have been reported in a number of studies, which were dependent on the HT22 cell line used (43-45). Glutamate induced necrosis at relatively early time points (before 12 h) and apoptosis at late time points (12-24 h) in HT22 cells (46). Mitochondrial oxidative stress and dysfunction were identified as essential events required for the induction of apoptosis. However, apoptosis occurs in HT22 cells through an ATP-independent process, involving the release of mitochondrial AIF, which catalyzes DNA fragmentation (46). Data from our previous study demonstrated that the parent compound, B355252, inhibits the glutamate-induced increase in AIF (18), which suggests that B355227 may protect HT22 from cell death by partially modulating AIF activity.

ROS plays a central role in glutamate-mediated oxidative stress and displays a synergistic association with Erk1/2 (47). However, in ischemia, Erk1/2 plays key roles in both the survival and apoptosis of cells, depending on the time and concentration of glutamate exposure (48,49). In the present study, an increase in the levels of Erk1/2 phosphorylation was revealed following 24 h glutamate exposure. Moreover, Erk1/2 phosphorylation was markedly reduced following B355227 co-exposure, suggesting an apoptotic role of Erk1/2. Consistent with the results of previous studies, the present study reported that the levels of p-Erk1/2 were increased following glutamate treatment in HT22 cells, leading to cell death (18,49,50). Following treatment with B355227, the phosphorylation of Erk1/2 decreased, leading to an increase in the levels of cell survival. Furthermore, an increase in the levels of ROS is associated with the levels of JNK and p38 phosphorylation, leading to apoptosis and cell death (15). Increased JNK phosphorylation in ischemia is associated with neurodegenerative diseases, and the corresponding inhibition was associated with neuroprotection (51). In the present study, the glutamate-induced increase in the phosphorylation of JNK in HT22 cells was reversed following co-exposure to B355227, thus protecting the cells from glutamate neurotoxicity. In addition, a decrease in levels of phosphorylated JNK and p38 was observed in cells treated with B355227 alone. The results of our previous study demonstrated that B355252 stimulated cell proliferation in cells treated with B355252 alone (18). Although the specific mechanisms underlying the observed increase in cell proliferation are yet to be elucidated, regulation of JNK and P38 may play a key role in the process. Thus, further research is required to understanding the underlying mechanisms.

The results of the present study demonstrated that the ratio of Bax/Bcl-2 was increased in cells following glutamate treatment, as a result of decreased levels of Bcl-2. In contrast, the ratio of Bax/Bcl-2 in HT22 cells exposed to B355227 alone, or co-treated with B355227 and glutamate was similar to that observed in the control group. Thus, the neuroprotective effects of B355227 may also be partially mediated by an increase in the anti-apoptotic Bcl-2 protein, or an interference with the mechanisms underlying the reduction of Bcl-2 following exposure to glutamate. Changes in anti-apoptotic protein expression levels have been observed in neuronal cell models of glutamate-induced neurotoxicity, and in animal models of ischemic stroke exposed to small molecules and extracts of medicinal plants with antioxidant and neuroprotective properties (52,53). The suppression of Ca^{2+} and subsequent decreases in the levels of JNK and p38 phosphorylation, coupled with the differential regulation of Bax/Bcl-2 expression highlight the neuroprotective attributes of B355227.

In conclusion, the findings of the present study demonstrate that B355227 is permeable *in vitro*, and exerts protection against glutamate-induced neurotoxicity through antioxidant and anti-apoptotic activities. These activities include a decrease in the levels of ROS, an increase in the levels of GSH, maintenance of intracellular Ca^{2+} homeostasis, prevention of the collapse of the MMP, reduction of Bcl-2 expression levels and modulation of the phosphorylation of MAPK- associated proteins in the cell. Collectively, the results of the present study revealed the neuroprotective nature of B355227, and highlighted it as a potential therapeutic compound to target oxidant-dependent mechanisms underlying disorders of the central nervous system.

Acknowledgements

Not applicable.

Funding

The present study was supported by the National Institutes of General Medical Sciences of the National Institutes of Health (grant no. SC3GM116667).

Availability of data and materials

The datasets used and/or analyzed during the current study are available from the corresponding author on reasonable request.

Authors' contributions

GCI and SP conceived and designed the experiments. SP and NSG performed the experiments. SP and GCI analyzed the data and wrote the manuscript. SP and GCI confirmed the authenticity of all the raw data. ALW and SRD synthesized the small molecule B355227 used in the study. All authors have read and approved the final manuscript.

Ethics approval and consent to participate

Not applicable.

Patient consent for publication

Not applicable.

Competing interests

The authors declare that they have no competing interests.

References

1. Barthels D and Das H: Current advances in ischemic stroke research and therapies. Biochim Biophys Acta Mol Basis Dis 1866: 165260, 2020.
2. Lee CH and Lee SH: General facts of stroke. In: Stroke Revisited: Pathophysiology of Stroke: From Bench to Bedside. Lee SH (ed). Springer, Singapore, pp3-10, 2020.

3. Deb P, Sharma S and Hassan KM: Pathophysiologic mechanisms of acute ischemic stroke: An overview with emphasis on therapeutic significance beyond thrombolysis. Pathophysiology 17: 197-218, 2010.
4. Mergenthaler P, Dirnagl U and Meisel A: Pathophysiology of stroke: Lessons from animal models. Metab Brain Dis 19: 151-167, 2004.
5. Jansson LC and Åkerman KE: The role of glutamate and its receptors in the proliferation, migration, differentiation and survival of neural progenitor cells. J Neural Transm (Vienna) 121: 819-836, 2014.
6. McEntee WJ and Crook TH: Glutamate: Its role in learning, memory, and the aging brain. Psychopharmacology (Berl) 111: 391-401, 1993.
7. Foran E and Trotti D: Glutamate transporters and the excitotoxic path to motor neuron degeneration in amyotrophic lateral sclerosis. Antioxid Redox Signal 11: 1587-1602, 2009.
8. Bridges RJ, Natale NR and Patel SA: System xc^- cystine/glutamate antiporter: An update on molecular pharmacology and roles within the CNS. Br J Pharmacol 165: 20-34, 2012.
9. Shih AY, Erb H, Sun X, Toda S, Kalivas PW and Murphy TH: Cystine/glutamate exchange modulates glutathione supply for neuroprotection from oxidative stress and cell proliferation. J Neurosci 26: 10514-10523, 2006.
10. Angelova PR, Vinogradova D, Neganova ME, Serkova TP, Sokolov VV, Bachurin SO, Shevtsova EF and Abramov AY: Pharmacological sequestration of mitochondrial calcium uptake protects neurons against glutamate excitotoxicity. Mol Neurobiol 56: 2244-2255, 2019.
11. Meredith GE, Totterdell S, Beales M and Meshul CK: Impaired glutamate homeostasis and programmed cell death in a chronic MPTP mouse model of Parkinson's disease. Exp Neurol 219: 334-340, 2009.
12. Nozaki K, Nishimura M and Hashimoto N: Mitogen-activated protein kinases and cerebral ischemia. Mol Neurobiol 23: 1-19, 2001.
13. Satoh T, Nakatsuka D, Watanabe Y, Nagata I, Kikuchi H and Namura S: Neuroprotection by MAPK/ERK kinase inhibition with U0126 against oxidative stress in a mouse neuronal cell line and rat primary cultured cortical neurons. Neurosci Lett 288: 163-166, 2000.
14. Shioda N, Han F and Fukunaga K: Role of Akt and ERK signaling in the neurogenesis following brain ischemia. Int Rev Neurobiol 85: 375-387, 2009.
15. Chen RW, Qin ZH, Ren M, Kanai H, Chalecka-Franaszek E, Leeds P and Chuang DM: Regulation of c-Jun N-terminal kinase, p38 kinase and AP-1 DNA binding in cultured brain neurons: Roles in glutamate excitotoxicity and lithium neuroprotection. J Neurochem 84: 566-575, 2003.
16. Williams AL, Dandepally SR, Gilyazova N, Witherspoon SM and Ibeanu G: Microwave-assisted synthesis of 4-chloro-N-(naphthalen-1-ylmethyl)-5-(3-(piperazin-1-yl)phenoxy)thiophene-2-sulfonamide (B-355252): A new potentiator of Nerve Growth Factor (NGF)-induced neurite outgrowth. Tetrahedron 66: 9577-9581, 2010.
17. Chimeh U, Zimmerman MA, Gilyazova N and Li PA: B355252, a novel small molecule, confers neuroprotection against cobalt chloride toxicity in mouse hippocampal cells through altering mitochondrial dynamics and limiting autophagy induction. Int J Med Sci 15: 1384-1396, 2018.
18. Gliyazova NS, Huh EY and Ibeanu GC: A novel phenoxy thiophene sulphonamide molecule protects against glutamate evoked oxidative injury in a neuronal cell model. BMC Neurosci 14: 93, 2013.
19. Gliyazova NS and Ibeanu GC: The chemical molecule B355252 is neuroprotective in an in vitro model of Parkinson's disease. Cell Mol Neurobiol 36: 1109-1122, 2016.
20. Pokharel S, Kamli MR, Mir BA, Malik A, Lee EJ and Choi I: Expression of transthyretin during bovine myogenic satellite cell differentiation. In Vitro Cell Dev Biol Anim 50: 756-765, 2014.
21. Pokharel S, Lee CH, Gilyazova N and Ibeanu GC: Analysis of gene expression and neuronal phenotype in neuroscreen-1 (NS-1) Cells. Int J Biomed Investig 1: 1-13, 2018.
22. Brown RC, Morris AP and O'Neil RG: Tight junction protein expression and barrier properties of immortalized mouse brain microvessel endothelial cells. Brain Res 1130: 17-30, 2007.
23. Birben E, Sahiner UM, Sackesen C, Erzurum S and Kalayci O: Oxidative stress and antioxidant defense. World Allergy Organ J 5: 9-19, 2012.
24. Baquer NZ, Taha A, Kumar P, McLean P, Cowsik SM, Kale RK, Singh R and Sharma D: A metabolic and functional overview of brain aging linked to neurological disorders. Biogerontology 10: 377-413, 2009.
25. Görlach A, Bertram K, Hudecova S and Krizanova O: Calcium and ROS: A mutual interplay. Redox Biol 6: 260-271, 2015.
26. Feno S, Butera G, Vecellio Reane D, Rizzuto R and Raffaello A: Crosstalk between Calcium and ROS in Pathophysiological Conditions. Oxid Med Cell Longev 2019: 9324018, 2019.
27. Kumari S, Mehta SL and Li PA: Glutamate induces mitochondrial dynamic imbalance and autophagy activation: Preventive effects of selenium. PLoS One 7: e39382, 2012.
28. Singer CA, Figueroa-Masot XA, Batchelor RH and Dorsa DM: The mitogen-activated protein kinase pathway mediates estrogen neuroprotection after glutamate toxicity in primary cortical neurons. J Neurosci 19: 2455-2463, 1999.
29. Yamazaki Y, Arita K, Harada S and Tokuyama S: Activation of c-Jun N-terminal kinase and p38 after cerebral ischemia upregulates cerebral sodium-glucose transporter type 1. J Pharmacol Sci 138: 240-246, 2018.
30. Pardridge WM: Drug transport across the blood-brain barrier. J Cereb Blood Flow Metab 32: 1959-1972, 2012.
31. Banks WA: Characteristics of compounds that cross the blood-brain barrier. BMC Neurol 9 (Suppl 1): S3, 2009.
32. Koto T, Takubo K, Ishida S, Shinoda H, Inoue M, Tsubota K, Okada Y and Ikeda E: Hypoxia disrupts the barrier function of neural blood vessels through changes in the expression of claudin-5 in endothelial cells. Am J Pathol 170: 1389-1397, 2007.
33. Yang S, Mei S, Jin H, Zhu B, Tian Y, Huo J, Cui X, Guo A and Zhao Z: Identification of two immortalized cell lines, ECV304 and bEnd3, for in vitro permeability studies of blood-brain barrier. PLoS One 12: e0187017, 2017.
34. Stamatovic SM, Johnson AM, Keep RF and Andjelkovic AV: Junctional proteins of the blood-brain barrier: New insights into function and dysfunction. Tissue Barriers 4: e1154641, 2016.
35. Katsuno T, Umeda K, Matsui T, Hata M, Tamura A, Itoh M, Takeuchi K, Fujimori T, Nabeshima Y, Noda T, *et al*: Deficiency of zonula occludens-1 causes embryonic lethal phenotype associated with defected yolk sac angiogenesis and apoptosis of embryonic cells. Mol Biol Cell 19: 2465-2475, 2008.
36. Belov Kirdajova D, Kriska J, Tureckova J and Anderova M: Ischemia-triggered glutamate excitotoxicity from the perspective of glial cells. Front Cell Neurosci 14: 51, 2020.
37. Atlante A, Calissano P, Bobba A, Giannattasio S, Marra E and Passarella S: Glutamate neurotoxicity, oxidative stress and mitochondria. FEBS Lett 497: 1-5, 2001.
38. Kho AR, Choi BY, Lee SH, Hong DK, Lee SH, Jeong JH, Park KH, Song HK, Choi HC and Suh SW: Effects of protocatechuic acid (PCA) on global cerebral ischemia-induced hippocampal neuronal death. Int J Mol Sci 19: 19, 2018.
39. Chen GJ and Yang MS: The effects of calcium channel blockers in the prevention of stroke in adults with hypertension: A meta-analysis of data from 273,543 participants in 31 randomized controlled trials. PLoS One 8: e57854, 2013.
40. Ha JS and Park SS: Glutamate-induced oxidative stress, but not cell death, is largely dependent upon extracellular calcium in mouse neuronal HT22 cells. Neurosci Lett 393: 165-169, 2006.
41. Abramov AY and Duchen MR: Mechanisms underlying the loss of mitochondrial membrane potential in glutamate excitotoxicity. Biochim Biophys Acta 1777: 953-964, 2008.
42. Tait SW and Green DR: Mitochondria and cell death: Outer membrane permeabilization and beyond. Nat Rev Mol Cell Biol 11: 621-632, 2010.
43. Park JS, Park JH and Kim KY: Neuroprotective effects of myristargenol A against glutamate-induced apoptotic HT22 cell death. RSC Advances 9: 31247-31254, 2019.
44. Tan S, Wood M and Maher P: Oxidative stress induces a form of programmed cell death with characteristics of both apoptosis and necrosis in neuronal cells. J Neurochem 71: 95-105, 1998.
45. Weon JB, Yun BR, Lee J, Eom MR, Ko HJ, Lee HY, Park DS, Chung HC, Chung JY and Ma CJ: Neuroprotective effect of steamed and fermented *Codonopsis lanceolata*. Biomol Ther (Seoul) 22: 246-253, 2014.
46. Fukui M, Song JH, Choi J, Choi HJ and Zhu BT: Mechanism of glutamate-induced neurotoxicity in HT22 mouse hippocampal cells. Eur J Pharmacol 617: 1-11, 2009.
47. Levinthal DJ and Defranco DB: Reversible oxidation of ERK-directed protein phosphatases drives oxidative toxicity in neurons. J Biol Chem 280: 5875-5883, 2005.
48. Kim SH, Kim KY, Park SG, Yu SN, Kim YW, Nam HW, An HH, Kim YW and Ahn SC: Mitochondrial ROS activates ERK/autophagy pathway as a protected mechanism against deoxypodophyllotoxin-induced apoptosis. Oncotarget 8: 111581-111596, 2017.

49. Sato K, Yamanaka Y, Asakura Y and Nedachi T: Glutamate levels control HT22 murine hippocampal cell death by regulating biphasic patterns of Erk1/2 activation: Role of metabolic glutamate receptor 5. Biosci Biotechnol Biochem 80: 712-718, 2016.
50. Stanciu M, Wang Y, Kentor R, Burke N, Watkins S, Kress G, Reynolds I, Klann E, Angiolieri MR, Johnson JW, *et al*: Persistent activation of ERK contributes to glutamate-induced oxidative toxicity in a neuronal cell line and primary cortical neuron cultures. J Biol Chem 275: 12200-12206, 2000.
51. Yang DD, Kuan CY, Whitmarsh AJ, Rincón M, Zheng TS, Davis RJ, Rakic P and Flavell RA: Absence of excito-toxicity-induced apoptosis in the hippocampus of mice lacking the Jnk3 gene. Nature 389: 865-870, 1997.
52. Lee HJ, Spandidos DA, Tsatsakis A, Margina D, Izotov BN and Yang SH: Neuroprotective effects of *Scrophularia buergeriana* extract against glutamate-induced toxicity in SH-SY5Y cells. Int J Mol Med 43: 2144-2152, 2019.
53. Zhang G, Zhang T, Wu L, Zhou X, Gu J, Li C, Liu W, Long C, Yang X, Shan L, *et al*: Neuroprotective effect and mechanism of action of tetramethylpyrazine nitrone for ischemic stroke therapy. Neuromolecular Med 20: 97-111, 2018.